PAPER

Non-dipole effect in vortex high-order harmonic generation

To cite this article: Bincheng Wang *et al* 2020 *J. Phys. B: At. Mol. Opt. Phys.* **53** 215601

View the article online for updates and enhancements.

Non-dipole effect in vortex high-order harmonic generation

Bincheng Wang[1] [iD]**, Liang Li[1], Yinfu Zhang[1], Chunyang Zhai[1], Xiaosong Zhu[1], Pengfei Lan[1] and Peixiang Lu[1,2,*]**

[1] School of Physics and Wuhan National Laboratory for Optoelectronics, Huazhong University of Science and Technology, Wuhan 430074, People's Republic of China
[2] Laboratory of Optical Information Technology, Wuhan Institute of Technology, Wuhan 430205, People's Republic of China

E-mail: pengfeilan@hust.edu.cn and lupeixiang@hust.edu.cn

CrossMark

Abstract
We discuss the non-dipole effect in high-order harmonic generation from atoms driving by a linearly polarized vortex beam. Different from the selection rule under the dipole approximation, where only odd high harmonics are allowed, both even and odd harmonics are generated in the vortex beam. Moreover, the polarization states of the harmonics are modulated. Elliptically polarized high harmonics can be directly generated with a linearly polarized vortex beam. We show that these non-dipole effects arise from the orbital angular momentum and spin angular momentum of the vortex beam.

Keywords: high-order harmonic generation, multiphoton ionization and excitation to highly excited states, photon interactions with atoms

(Some figures may appear in colour only in the online journal)

1. Introduction

Angular momentum is a fundamental property of light, similar to energy and linear momentum. In paraxial condition, it can be split into a spin part called spin angular momentum (SAM), and an orbital part called orbital angular momentum (OAM) [1, 2]. Macroscopically, the OAM of light manifests itself in the spatial properties of the light and the SAM refers to the helicity of the light. One of the most widely used beams with well-defined OAM and SAM is the vortex beam which has an azimuthal phase dependence of $e^{il\phi}$, where l is the topological charge and ϕ is the azimuthal angle [3, 4]. Due to its OAM, the vortex beam has attracted a great deal of attention in optical communication [5], micromanipulation [6, 7], and quantum optics [8, 9]. In these applications, the large OAM plays an important role. For example, in optical communication, the OAM of the vortex beam can provide an extra degree of freedom for communication and, with the OAM increasing, the capacity of communication systems can be

increased [5]. Recently, some researchers find that utilizing a nonlinear light–matter interaction called high-order harmonic generation (HHG), a tunable extreme-ultraviolet (XUV) vortex beam with high topological charge can be obtained [10–14]. On the other hand, as light–matter interaction inherently includes the exchange of angular momentum, the investigation of vortex HHG has great significance in revealing the underlying physical property of the angular momentum of light [15–19].

HHG is usually understood by the three-steps model [20]. First, the electron is freed by a strong laser field. Then it is accelerated and oscillated in the laser field. Finally, when the electron approaches the parent ion, it recombines and the energy obtained in the laser field is emitted as the form of high-order harmonics. According to the three-steps model, the maximum speed of the recombination electron is E_0/ω_0, where ω_0 and E_0 are the frequency and maximum electric amplitude of the laser field. The maximum range of the electron motion is $\pm E_0/\omega_0^2$. One can see that for a typical near IR laser with the intensity of 3×10^{14} W cm^{-2} and the wavelength of 1600 nm, the maximum range $E_0/\omega_0^2 \sim 3.18$ nm which is much smaller

than the wavelength of the driving laser. Therefore, in general, the spatial form of the laser field is neglected, i.e., the vector potential $A(r, t)$ (and also the electric field $E(r, t)$) can be regarded as $A(r, t) = A(t)$, which is called the dipole approximation [21–23]. In particular, theoretical models of strong-field physics build heavily on this approximation and it usually works well for most commonly used laser sources [24–29]. However, because the magnetic field component of the Lorentz force acting on the electron depends linearly on the electron's velocity $v_e \propto E_0/\omega_0$, high-velocity electrons can be strongly influenced by the magnetic field [30]. When the laser field is in the mid-infrared region, e.g., 3.4 μm, the speed of the electron motion is so large that the dipole approximation is expected to be broken down. Recently, some phenomena related to the breakdown of the dipole approximation have been investigated [30–33], such as a momentum shift in the photon ionization process under the 3.4 μm driving laser [30]. Nevertheless, it is generally considered that the dipole approximation works well in the near IR region [16, 17].

In this paper, we focus on the interaction of a single atom with the vortex beam. Different from the gauss beam, the vortex beam has a rotational phase in space. This rotational phase will bring a spatial structure variation of the electric field and induce a non-dipole effect in HHG. It is shown that, with the topological charge increasing, although the maximum range of the electron motion is still much smaller than the wavelength of the laser field, the spatial phase of the laser electric field varies very fast and cannot be neglected anymore. In this case, the dipole approximation is broken down. In a vortex beam with a high topological charge, the selection rule of HHG and the polarization of harmonics are changed: (i) both odd and even harmonics can be generated driven by a linearly polarized vortex beam. In contrast, only odd harmonics can be generated under the dipole approximation. (ii) The polarization of the high-order harmonics are also modulated. The high-order harmonics are no longer linearly polarized but elliptically polarized.

2. Theoretical model

At first, we discuss the physical model we used here. In the Coulomb gauge, the vector potential of the vortex beam has three non-zero polarization components that are in the polarization plane and the propagation direction. These components will lead to different non-dipole effects in the polarization plane and the propagation direction [30, 31], allowing us to study them separately [15]. In this paper, we focus on the non-dipole effect in the polarization plane which is induced by the phase gradient of the electric field.

We consider the interaction of a hydrogen atom with ultrashort vortex pulses. The 2D TDSE describing the dynamics of the electron beyond the dipole approximation is

$$i\hbar \frac{\partial}{\partial t} \psi(r, t) = -\frac{\hbar^2}{2m} \left[\frac{1}{2}(p - A(r, t))^2 + V(r) \right] \psi(r, t), \quad (1)$$

where $\psi(r, t)$ is the electron wavefunction, p is the momentum operator, $A(r, t)$ is the vector potential of the laser field

(atomic units are used). $V(r)$ is the Coulomb potential which is modeled by a softcore potential:

$$V(r) = -\frac{1}{\sqrt{r^2 + b}}. \quad (2)$$

b is the softcore parameter, which is 0.63 for the hydrogen atom. The above TDSE can be numerically solved as [34, 35].

The spatial profile of the driving vortex pulse is an Laguerre–Gaussian (LG) mode:

$$\mathrm{LG}_{l,m}(\rho, \phi, z) = E_0 \frac{W_0}{W(z)} \left(\frac{\rho}{W(z)} \right)^l \mathrm{L}_m^{|l|} \left[\frac{2\rho^2}{W^2(z)} \right]$$
$$\times \exp \left(-\frac{\rho^2}{W^2(z)} \right)$$
$$\times \exp \left(ik\frac{\rho^2}{2R(z)} + i\xi(z) + il\phi \right). \quad (3)$$

$W(z)$ is the beam width. $R(z)$ is the wave front radius of curvature, given by $R(z) = z[1 + (\frac{z_0}{z})^2]$. $\xi(z)$ is the gouy phase and k is the wave number. $\mathrm{L}_m^{|l|}[x]$ is the associated Laguerre polynomial. The indices $l = 0, \pm 1, \pm 2, \ldots$ and $m = 0, 1, 2, \ldots$ correspond to the topological charge and the number of radial nodes of the mode, respectively.

The angular momentum of light is defined as [36, 37]:

$$J = \int \vec{z} \times \left(\vec{E} \times \vec{B} \right) \mathrm{d}r. \quad (4)$$

Substituting the vortex beam (LG mode) into equation (4), the OAM and SAM are described as:

$$\mathrm{OAM} = \int i\omega \frac{\varepsilon_0}{2} (\mathrm{LG}^* \nabla \mathrm{LG} - \mathrm{LG} \nabla \mathrm{LG}^*) \mathrm{d}r, \quad (5)$$

and

$$\mathrm{SAM} = \int \frac{\pm\omega}{2} \frac{\partial |\mathrm{LG}|^2}{\partial \rho} \hat{\phi} \, \mathrm{d}r. \quad (6)$$

It is worth noting that the OAM and SAM mentioned here are not themselves angular momentum, but refer to the orbital and spin parts of the angular momentum [37] (although common practice almost requires us to refer to them as the OAM and SAM).

The temporal envelope of the light pulse is a trapezoid with the total pulse duration of 10 optical cycles with 2 cycles on and off. The light pulse is linearly polarized, the wavelength of the pulse is 1600 nm and the intensity is 3×10^{14} W cm^{-2}. The spatial profile of the beam is a vortex beam with the waist radius $W(0)$ is 30 μm. We only change the topological charge of the laser field and the position of the atom.

The high-order harmonics are obtained from the time-dependent dipole acceleration:

$$s_{x,y}(\omega) = |\mathcal{F}[a_{x,y}(t)]|^2, \quad (7)$$

where $\mathcal{F}$ represents the fourier transform. The dipole acceleration $a_{x,y}(t)$ is obtained by the Ehrenfest method:

$$a_x(t) = \langle \psi(t) \left| \frac{\partial(V(r) + E(r,t))}{\partial x} \right| \psi(t) \rangle.$$

$$a_y(t) = \langle \psi(t) \left| \frac{\partial(V(r) + E(r,t))}{\partial y} \right| \psi(t) \rangle. \qquad (8)$$

The high-order harmonic spectra can also be spilt into right-handed and left-handed spectra which are calculated by [38]:

$$s_\pm = |a_\pm|^2 = \left| \frac{1}{\sqrt{2}} \mathcal{F}[(a_x(t) \pm ia_y(t))] \right|^2, \qquad (9)$$

where $a_\pm$ are the right-handed and left-handed components of the harmonic electric fields. The ellipticity of the harmonics is:

$$\varepsilon = \frac{(|a_+| - |a_-|)}{(|a_+| + |a_-|)}. \qquad (10)$$

3. The generation of even harmonics

In figure 1(a), we show the harmonic spectra generated from the vortex beam. The topological charge of the vortex beam is 200 [39, 40]. The pink one is obtained under the dipole approximation [$A(r,t) = A(t)$] and the blue one is calculated beyond the dipole approximation [$A(r,t) = A(r,t)$]. One can see that these harmonic spectra have similar structures, such as a plateau and a cutoff at the same order. However, the selection rule of HHG, i.e., the allowed high-order harmonics, is different dramatically. For clarity, figure 1(b) displays the detailed structure of the harmonic spectra in the range of 42nd to 55th. In contrast with the result under the dipole approximation, where only odd harmonics can be generated, the harmonic spectra beyond the dipole approximation have both odd and even harmonics, i.e., the normal selection rule is broken [41].

According to the theory of the HHG [42, 43], the generation of the qth order harmonic is limited by the conservation law of energy, i.e. $\omega_q = q\omega_0$, where ω_0 and ω_q are the frequency of the fundamental light and the qth harmonic. Besides, under the dipole approximation, the spatial structure of the laser beam is neglected and the total system has space-reflection invariance. Therefore, the HHG should also follow the conservation law of parity. Only odd photons can be absorbed and there are only odd harmonics [18, 41]. However, in the condition beyond the dipole approximation, the laser field has a complex spatial form and the space-reflection invariance of the total system is broken down. The selection rule will not be limited by the conservation law of parity and both the odd and even harmonics are allowed.

In figure 2(b), we display the average intensities of the even (blue circles) and odd (red squares) harmonics as a function of the topological charge *l*. The average intensities of the even and odd harmonics are calculated by adding up the intensities of the even and odd harmonics. One can see that when the topological charge is zero, the average intensity of the even harmonics is one order of magnitude lower than that of the odd harmonics. With the topological charge increasing, the even harmonics is increased. When the topological charge is 15, the average intensity of even harmonic is 1/3 of the odd harmonic, which can be detected in experiment. When the topological
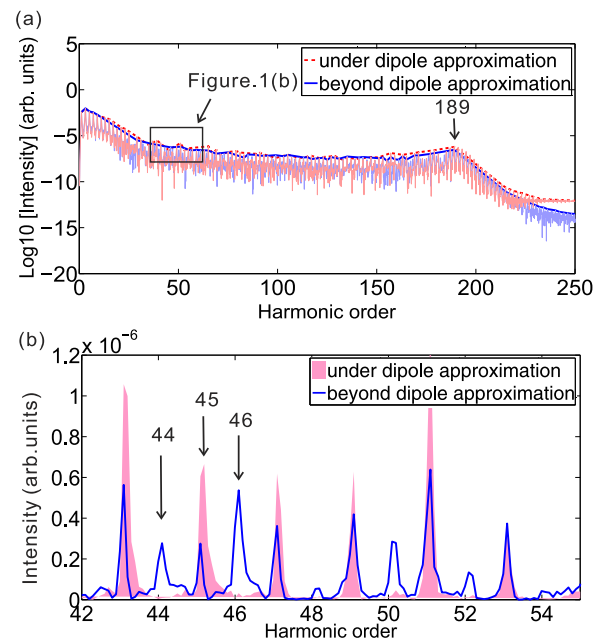

Figure 1. (a) The comparison of the harmonic spectra under the dipole approximation and beyond the dipole approximation. The atom is placed at the position where the light beam is strongest [indicated by the square (b) in figure 2(a)] and the position along the propagation direction is $z = 0$ (b) the detailed structure of harmonic spectra from the order of 42nd to 55th.

charge is greater than 100, the odd and even harmonics are comparable.

In figure 2(c), we illustrate the average intensities of the odd and even harmonics (red squares and blue circles, respectively) as a function of the radial position of the atom, where the topological charge is 10. We choose different radial positions along the arrow (c) and calculate the high-order harmonics. To focus on the relation between the non-dipole effect and the position of the atom only, the intensity of the vortex beam is adjusted to 3×10^{14} W cm^{-2} at the atom vicinity as in reference [15]. The peak laser intensity at the optical axis is increased with the atom closing to the center of the laser beam. While the radial distance is 10 μm, the laser intensity is 3×10^{15} W cm^{-2} and while the radial distance is 6 μm, it is about 3×10^{17} W cm^{-2}. Figure 2(c) shows that the intensity of the odd harmonics is independent of the radial position. On the contrary, the intensity of the even harmonics is increased with the radial position changing from 14 μm to 1 μm. In the range of 14 μm to 8μm, the intensity of the even harmonics is increased slowly. In the range of 8 μm to 1 μm, the intensity increases very fast.

These phenomena are related to the variation of the laser spatial structure. According to the previous research about the OAM [44, 45], a vortex beam with the topological charge *l* has the OAM of $l\hbar$. Besides, we can define a local OAM which is corresponding to the ratio of the OAM to the energy density. This definition is based on a semiclassical interpretation and the OAM in the beam can be written as the integral over the local OAM. In the three-steps model of HHG, the harmonics only can be generated by the electrons that are recombined with parent ion. The maximum motion range of these electrons are E_0/ω_0^2. Accordingly, to investigate the influence
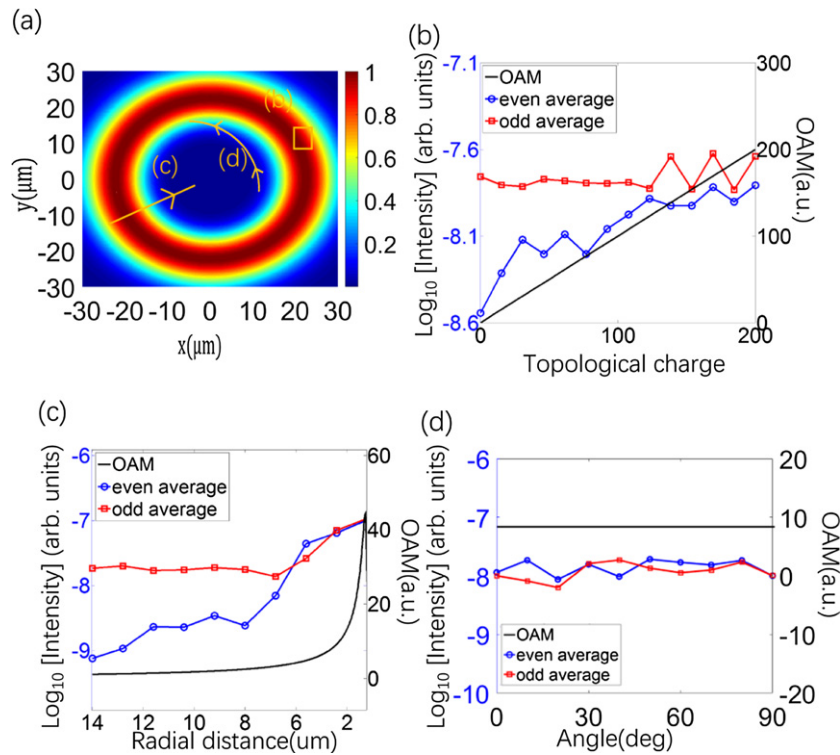
Figure 2. (a) The intensity distribution of the vortex beam at $z = 0$. The square (b), arrow (c) and arrow (d) indicate the variation of figures (b), (c), and (d). (b) The average intensity of harmonics as a function of the topological charge when the radial distance of the atom is 14 μm and the angular position is 45°. (c) The average intensity of harmonic and the EM-LOAM when the radial distance of the atom is changed from 14 μm to 1 μm, the angular position is 45° and the topological charge is 10. (d) The average intensity of harmonic and the EM-LOAM when the angular position of the atom varies from 0° to 90°, the radial distance is 7 μm and the topological charge is 10.

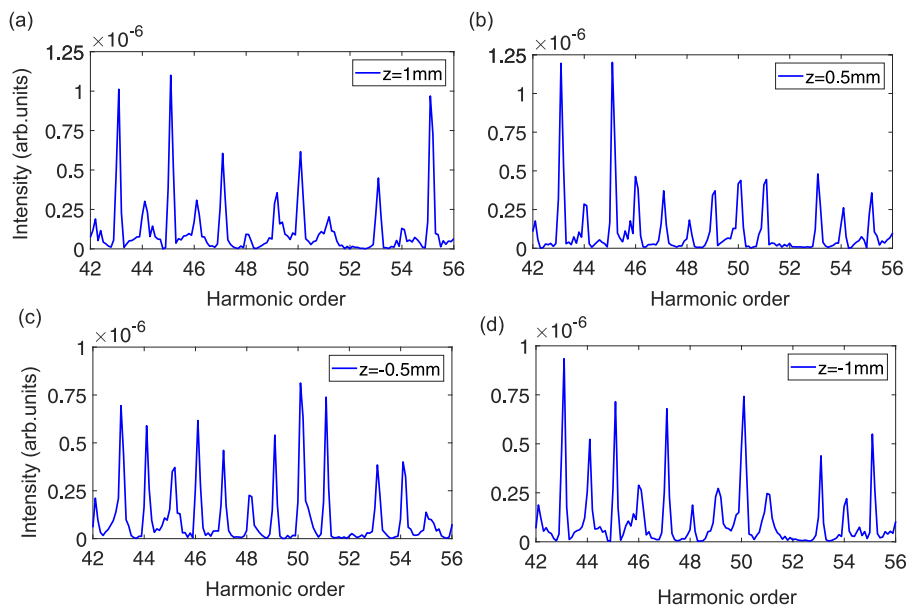**Figure 3.** (a)–(d) The harmonic spectra from the order of 42nd to 55th when the atom is placed at $z = -1$ mm, -0.5 mm, 0.5 mm and 1 mm.

of the laser spatial structure variation for HHG in this electron motion region, we can define an electron motion local OAM and SAM (EM-LOAM and EM-LSAM, respectively) as an integral of the local OAM and SAM over the electron motion range [36].

We calculate the EM-LOAM and display it as a function of the radial position (black line) in figure 2(c). One can see

that with the atom approaching the center of the beam, the EM-LOAM is increased. In the range of 14 μm to 8 μm, the EM-LOAM is increased slowly. In the range of 8 μm to 1 μm, the EM-LOAM increases quickly. The variation of the EM-LOAM is consistent with the variation of the even harmonic intensity. Analogously, as shown in figure 2(d), when the angular position of the atom changes from 0° to 90° [arrow
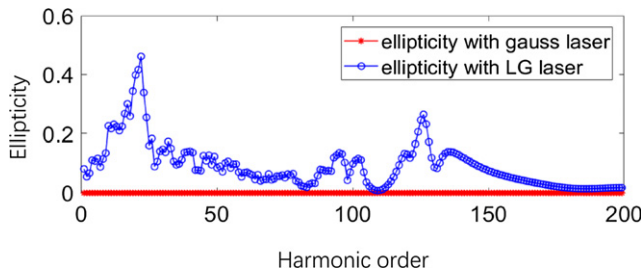
J. Phys. B: At. Mol. Opt. Phys. **53** (2020) 215601

B Wang *et al*

Figure 4. The harmonic ellipticity as a function of harmonic order.

(d) in figure 2(a)], the EM-LOAM is unchanged. This result well matches the variation of the even harmonic intensity.

As discussed in section 2, these non-dipole effects are induced by the EM-LOAM in the polarization plane. In different positions of the *z* axis (propagation direction), these effects are similar. To demonstrate it, in figure (3), we display the harmonic spectra in the range of 42nd to 55th, when the atom is placed at $z = 1$ mm, 0.5 mm, -0.5 mm, -1 mm and the position of the atom in the polarization plane is same with figure 1(a). Other laser parameters are the same as figure 1. It is shown that, when the atom is placed at different positions of the *z* axis, both the even and odd harmonics can also be generated, which agrees with the result of figure 1(b).

4. The generation of elliptically polarized harmonics

Besides the selection rule, the ellipticity of the high-order harmonics is also modulated due to the non-dipole effect. Figure 4 shows the generated harmonic ellipticity as the function of the harmonic order. The laser parameters are the same as those in figure 1 but the atom is placed at the radial position of 7 μm. The ellipticity is calculated based on equation (10). One can see that the generated harmonics are elliptically polarized, comparing with the harmonic obtained from the gauss beam whose ellipticity is zero. In the range of 15th to 30th, the ellipticity of the harmonic is increased from 0.2 to 0.5 which is larger than that in the plateau. In the plateau region, the ellipticity is about 0.2 and in the cutoff region ($>$100th), it is increased to 0.3.

Figure 5(a) shows the phase difference of the electron trajectories in the different recombination energies between the Gaussian laser beam and the LG laser beam. These phase represents a classical motion action calculated by [46]:

$$\phi = -\int_{t_0}^{\infty} \left[\frac{V(t)^2}{2} - \frac{Z}{r(t)} + I_{\mathrm{p}} \right] \mathrm{d}t, \tag{11}$$

where the t_0 is the ionization time, $V(t)$ is the speed and $r(t)$ is the position of the electron. One can see that in the range of 15th to 30th, the phase changes very quickly and irregularly, which leads to the ellipticity in this range also varies very large (from 0.2 to 0.5). It means that the spatial variation of the vortex beam has a big influence on these electron trajectories. In the plateau, the phase difference is almost a constant corresponding to the unchanged ellipticity in this region. In the

cutoff region, the phase difference and the ellipticity decrease to zero.

Figure 5(b) shows the relation between the average ellipticity and the topological charge. One can see that the ellipticity of the odd and even harmonics varies around 0.1 and is not changed with the topological charge. In figure 5(c), we investigate the relationship between the ellipticity and the radial position of the atom. With the atom approaching the center of the beam, the ellipticity becomes larger [see in figure 5(c)]. In detail, in the range of 14 μm–4 μm, the ellipticity is only changed from 0 to -0.07. In the range of 4 μm–1 μm, the ellipticity of the odd (even) harmonics increases quickly from -0.07 to 0.44 (0.26). As shown in figure 5(d), when the angular position of the atom is changed from $0°$ to $90°$, the ellipticity of the plateau harmonic (from 30th to 100th) is almost unchanged. In figures 5(e) and (f), we calculate the classical action of the electron trajectories as the function of the recombination energy and the position of the atom. It can be found that the low order harmonics ($<$30th) are more sensitive to the spatial phase variation. In the radial direction, with the atom closing to the center of the beam, the phase of the plateau harmonic is increased and on the contrary, the phase of the low order harmonic is complicated. In the angular direction, the phase of the plateau harmonic is unchanged with the angle but the phase of the low order has some phase jump which leads to the generation of the large ellipticity harmonics.

Analogous to the EM-LOAM, we calculate the EM-LSAM in the range of the electron motion and display it (black line) as a function of the topological charge, radial position and angular position in figures 5(b)–(d), respectively. It is found that the variation of the harmonic ellipticity is consistent with the variation of the EM-LSAM. When the atom approaches the center of the beam, the EM-LSAM is increased. For example, when the radial position is 4 μm, the EM-LSAM is -0.25 a.u. and when the radial position is 1 μm, the EM-LSAM is up to approximately 5 a.u. Consequently, the ellipticity of the harmonics increases with the radial position decreasing. When the angular position of the atom is changed from $0°$ to $90°$, the EM-LSAM is a constant (1.25 a.u.). The ellipticity of the even and odd harmonics is also unchanged.

The origin of the elliptically polarized HHG can be attributed to the spatial phase of the vortex beam. To clarify this problem, we rewrite the qth order harmonic as:

$$
\begin{aligned}
a_x(q) &= \int a_x(t) e^{-iq\omega_0 t} \ \mathrm{d}t \\
&= \int \left\langle \psi(r,t) \left| \frac{\partial (V(r) + E(r,t))}{\partial x} \right| \psi(r,t) \right\rangle) \ e^{-iq\omega_0 t} \ \mathrm{d}t,
\end{aligned}
\tag{12}
$$

$$
\begin{aligned}
a_y(q) &= \int a_y(t) e^{-iq\omega_0 t} \ \mathrm{d}t \\
&= \int \left\langle \psi(r,t) \left| \frac{\partial (V(r) + E(r,t))}{\partial y} \right| \psi(r,t) \right\rangle) \ e^{-iq\omega_0 t} \ \mathrm{d}t.
\end{aligned}
\tag{13}
$$

In the dipole approximation, both $\partial E(r,t)/\partial x$ and $\partial E(r,t)/\partial y$ in equations (12) and (13) are zero. The whole system is
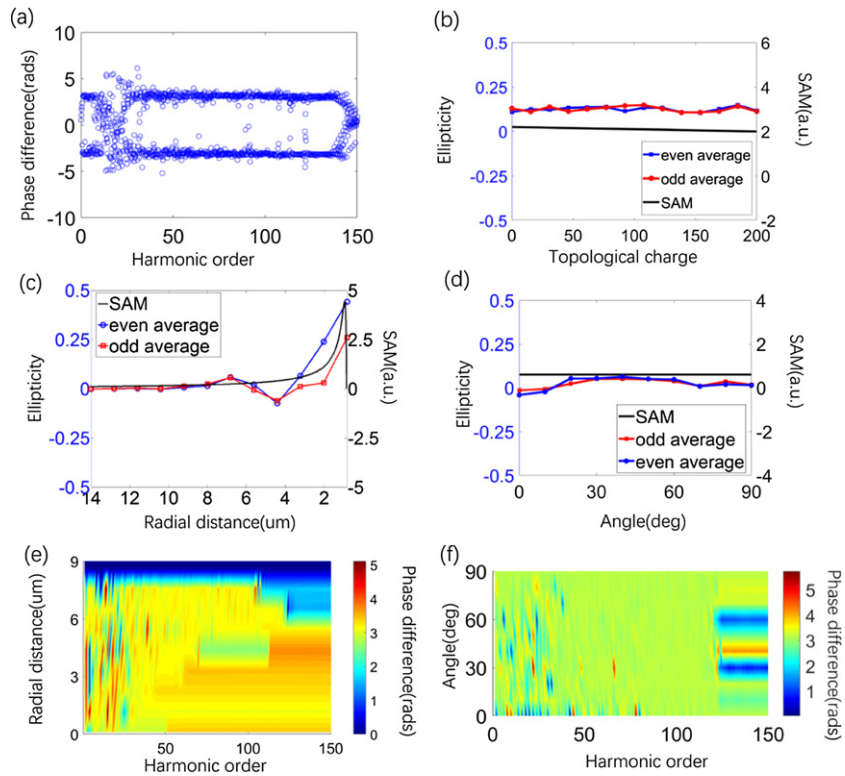
Figure 5. (a) The phase difference of the electron trajectories in the different recombination energies. (b) The average ellipticity and the EM-LSAM as a function of the topological charge when the radial distance of the atom is 7 μm and the angular position is 45°. (c) The average ellipticity and the EM-LSAM when the radial distance of the atom is changed from 14 μm to 1 μm, the angular position is 45° and the topological charge is 10. (d) The average ellipticity and the EM-LSAM when the angular position of the atom varies from 0° to 90°, the radial distance is 7 μm and the topological charge is 10. (e) The phase difference as a function of the recombination energy and the radial distance. (f) The phase difference as a function of the recombination energy and the angular position.
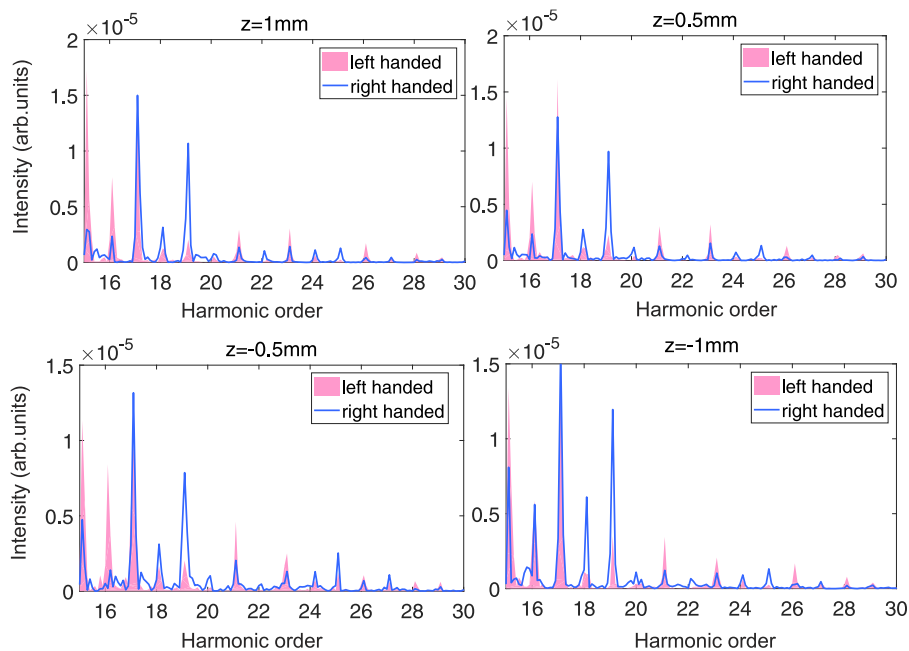

Figure 6. (a) The right-handed and left-handed harmonic spectra in the range of 15th to 30th when the atom is placed at $z = -1$ mm. (b) The right-handed and left-handed harmonic spectra in the range of 15th to 30th when the atom is placed at $z = -0.5$ mm. (c) The right-handed and left-handed harmonic spectra in the range of 15th to 30th when the atom is placed at $z = 0.5$ mm. (d) The right-handed and left-handed harmonic spectra in the range of 15th to 30th when the atom is placed at $z = 1$ mm.

J. Phys. B: At. Mol. Opt. Phys. **53** (2020) 215601

B Wang *et al*

symmetric in space. If the driving laser is linearly polarized along the *x* (or *y*) direction, the *y*-component (or *x*-component) of the generated high harmonics is zero, i.e., the polarization of HHG is same to the driving laser pulse. In contrast, if the spatial phase of the vortex beam varies very fast, the terms $\partial E(r,t)/\partial x$ and $\partial E(r,t)/\partial y$ is non-zero and will generate a corresponding *y*-component (or *x*-component) of the harmonics. The phase difference between *x*-component and *y*-component is decided by the terms $\partial E(r,t)/\partial x$ and $\partial E(r,t)/\partial y$, i.e. the EM-LSAM. It means that the generation of the elliptically polarized harmonics originates from the EM-LSAM of the vortex beam.

Moreover, in the same way, we display the right-handed and left-handed harmonic spectra in figure 6, when the atom is placed at different positions of *z* axis ($z = 1$ mm, 0.5 mm, -0.5 mm, -1 mm). Other laser parameters and atom position are the same as those in figure 4. It is found that the modulation of harmonic ellipticity can also be found in different positions of the *z* axis. 4.

5. Conclusion

In conclusion, we investigate the non-dipole effect of HHG in the vortex beam. Our results show that the EM-LOAM and EM-LSAM play an important role in the HHG. The EM-LOAM will lead to the breakdown of the selection rule and both even and odd high harmonics can be generated. The EM-LOAM will lead to the change of polarization. In a linearly polarized laser pulse, the generated harmonics are not linearly polarized but elliptically polarized. The ellipticity is increased with the EM-LSAM increasing. These results show that the EM-LOAM and EM-LSAM will result in noticeable non-dipole effects in vortex HHG.

Acknowledgment

ORCID iDs

Bincheng Wang https://orcid.org/0000-0002-8471-5585

References

[1] Allen L, Beijersbergen M W, Spreeuw R J C and Woerdman J P 1992 *Phys. Rev. A* **45** 8185
[2] Soskin M S and Vasnetsov M V 2001 *Prog. Opt.* **42** 219
[3] Yao A M and Padgett M J 2011 *Adv. Opt. Photon.* **3** 161
[4] Calvo G F, Picon A and Bagan E 2006 *Phys. Rev. A* **73** 013805
[5] Wang J *et al* 2012 *Nat. Photonics* **6** 488
[6] Padgett M and Bowman R 2011 *Nat. Photonics* **5** 343
[7] Grier D G 2003 *Nature* **424** 810
[8] Fickler R, Lapkiewicz R, Plick W N, Krenn M, Schaeff C, Ramelow S and Zeilinger A 2012 *Science* **338** 640
[9] Mair A, Vaziri A, Weihs G and Zeilinger A 2001 *Nature* **412** 313
[10] Gauthier D *et al* 2017 *Nat. Commun.* **8** 14971
[11] Kong F *et al* 2017 *Nat. Commun.* **8** 14970
[12] Hernández-García C, Picón A, San Román J and Plaja L 2013 *Phys. Rev. Lett.* **111** 083602
[13] Zhao X, Hui W, Yu W-W and Lin C D 2018 *Phys. Rev. A* **98** 053404
[14] Vieira J, Trines R M G M, Alves E P, Fonseca R A, Mendonça J T, Bingham R, Norreys P and Silva L O 2016 *Phys. Rev. Lett.* **117** 265001
[15] Picón A, Benseny A, Mompart J, Vázquez de Aldana J R, Plaja L, Calvo G F and Roso L 2010 *New J. Phys.* **12** 083053
[16] Rego L, Roman J S, Picon A, Plaja L and Hernandez-Garcia C 2016 *Phys. Rev. Lett.* **117** 163202
[17] Telnov D A and Chu S-I 2017 *Phys. Rev. A* **96** 033807
[18] Turpin A, Rego L, Picn A, San Romn J and Hernndez-Garca C 2017 *Sci. Rep.* **7** 43888
[19] Wang R, Zhang Q, Ran C, Cao W and Lu P 2020 *Opt. Lett.* **45** 1383
[20] Corkum P B 1993 *Phys. Rev. Lett.* **71** 1994
[21] Lewenstein M, Balcou P, Ivanov M Y, L'Huillier A and Corkum P B 1994 *Phys. Rev. A* **49** 2117
[22] Reiss H R 2014 *J. Phys. B: At. Mol. Opt. Phys.* **47** 204006
[23] Wei J, Xiong W, Xiao X, Peng L and Gong Q 2015 *Phys. Rev. Lett.* **115** 193001
[24] Milošević D B, Paulus G G, Bauer D and Becker W 2006 *J. Phys. B: At. Mol. Opt. Phys.* **39** R203 10.1088/0953-4075/39/14/r01
[25] Liu K, Li M, Xie W, Guo k., Luo S, Yan J, Zhou Y and Lu P 2020 *Opt. Express* **28** 12439
[26] Protopapas M, Keitel C H and Knight P L 1997 *Rep. Prog. Phys.* **60** 389
[27] Zhai C, Shao R, Lan P, Wang B, Zhang Y, Yuan H, Stephen N M, He L and Lu P 2020 *Phys. Rev. A* **101** 053407
[28] Ivanov M and Pisanty E 2014 *Nat. Photonics* **8** 501
[29] Han X, Wang K, Xing X, Wang M and Lu P 2018 *ACS Photonics* **5** 3970–6
[30] Ludwig A, Maurer J, Mayer B W, Phillips C R, Gallmann L and Keller U 2014 *Phys. Rev. Lett.* **113** 243001
[31] He P L, Lao D and He F 2017 *Phys. Rev. Lett.* **118** 163203
[32] Maurer J *et al* 2018 *Phys. Rev. A* **97** 013404
[33] Reiss H R 2008 *Phys. Rev. Lett.* **101** 043002
[34] De Aldana J R V, Roso L and Roso L 2002 *Laser Part. Beams* **20** 185
[35] Shao R, Zhai C, Zhang Y, Sun N, Cao W, Lan P and Lu P 2020 *Opt. Express* **28** 15874
[36] Allen L and Padgett M J 2000 *Opt. Commun.* **184** 67
[37] Stephen M B, Allen L, Robert P C, Claire R G, Miles J P, Fiona C S and Alison M Y 2016 *J. Opt.* **18** 064004
[38] Wang D, Zhu X, Li L, Zhang X, Liu X, Lan P and Lu P 2018 *Phys. Rev. A* **98** 053410
    Li L, Lan P, He L *et al* 2020 *Phys. Rev. Lett.* **124** 157403
[39] Chen Y, Fang Z-X, Ren Y-X, Gong L and Lu R-D 2015 *Appl. Opt.* **54** 8030
[40] Cojoc D, Kaulich B, Carpentiero A, Cabrini S, Businaro L and Di Fabrizio E 2006 *Microelectron. Eng.* **83** 1360
[41] Liu X, Zhu X, Li L, Li Y, Zhang Q, Lan P and Lu P 2016 *Phys. Rev. A* **94** 033410
[42] Gariepy G, Leach J, Kim K T, Hammond T J, Frumker E, Boyd R W and Corkum P B 2014 *Phys. Rev. Lett.* **113** 153901
[43] Li L, Lan P, He L, Zhu X, Chen J and Lu P 2018 *Phys. Rev. Lett.* **120** 223203
[44] Amaral A M, Falcão-Filho E L and de Araújo C B 2014 *Opt. Express* **22** 30315
[45] Ch´vez-Cerda S, Padgett M J, Allison I, New G H C, Gutierrez-Vega J C, ÓNeil A T, MacVicar I and Courtial J 2002 *J. Opt. B: Quantum Semiclassical Opt.* **4** S52
[46] Li M, Geng J, Liu H, Deng Y, Wu C, Peng L, Gong Q and Liu Y 2014 *Phys. Rev. Lett.* **112** 113002